Astron. Astrophys. 323, 513–523 (1997)

ASTRONOMY AND ASTROPHYSICS

Giants with infrared excess

H. Plets[1], **C. Waelkens**[1], **R.D. Oudmaijer**[2], **and L.B.F.M. Waters**[3]

[1] Instituut voor Sterrenkunde, Katholieke Universiteit Leuven, Celestijnenlaan 200 B, B-3001 Heverlee, Belgium (hansp@ster.kuleuven.ac.be; christoffel@ster.kuleuven.ac.be)
[2] Imperial College of Science, Technology and Medicine, Blackett Laboratory, Prince Consort Road, London, SW7 2BZ, UK (r.oudmaijer@ic.ac.uk)
[3] Sterrenkundig Instituut Anton Pannekoek, Universiteit van Amsterdam, Kruislaan 403, 1098 SJ Amsterdam, The Netherlands (rensw@astro.uva.nl)

Received 30 July 1996 / Accepted 6 January 1997

Abstract. We have correlated optical and infrared catalogs in order to extract a large sample of luminosity class III stars with known infrared flux densities. For a non-negligible fraction of G and K giants, a far-infrared excess emission was found, starting beyond 25 μm. An explanation in terms of present-day mass loss thus becomes unlikely, since the dust should then be warmer and the excess emission less far in the infrared. We believe that the far-infrared excesses of these objects, most likely first-ascent giants, are related to the Vega phenomenon. The dusty disks around these stars, gradually cooled down during their main-sequence phase, could be reheated once the star leaves the main sequence and enters the luminous post-main-sequence phase. The fairly large sample we constructed enables us to derive an estimation for the occurrence of excesses. This fraction of G or K giants with far-infrared excess appears to be distinctly smaller than among main-sequence stars. Since the higher radiation field of giants could lead to a larger evaporation rate of the circumstellar debris, this fact does not conflict with our hypothesis.

Key words: circumstellar matter – stars: evolution – stars: late-type – stars: statistics – infrared: stars

1. Introduction

The detection of circumstellar dust around many main-sequence stars, i.e. the Vega phenomenon, has been one of the highlights of the IRAS mission (e.g. Aumann et al. 1984). It is probable that these dust excesses are in some way related to the existence of large bodies, e.g. comets or planetesimals, around these stars, at typical distances of ten astronomical units and more from the star (e.g. Telesco and Knacke 1991). In fact, collisions with such larger bodies could be the source of the replenishment of the dust debris disk, which is required in view of the appreciable ages of the stars, that appear to be much older than the timescales of the various effects which cause the disappearance of the circumstellar disk that initially surrounded the star (e.g. Backman and Paresce 1993).

The similarity of the debris disk in Vega-like stars with the Kuiper belt in our solar system has been pointed out by several authors (Backman and Paresce 1993; Weissman 1995; Backman et al. 1995). The Kuiper belt, whose existence was anticipated by Edgeworth (1949) and Kuiper (1951), is a reservoir for short-period comets (Fernandez 1980), that extends beyond the orbit of Neptune to some 60 AU from the Sun (for a review, see Weissman 1995).

Jura (1990) first addressed the question what happens to Vega-like disks when the central star ends its evolution on the main sequence and proceeds as a red giant. From a study of IRAS observations of some 100 bright giants, mostly of spectral type G, he concluded that infrared (IR) excesses are much rarer for such stars than for their progenitor A-type main-sequence stars. These observations suggest that the increased luminosity of the stars has drastically contributed to evaporate the remaining cometary bodies in the circumstellar disks. On the other hand, Matese and Whitmire (1989) have suggested that the remaining small fragments could provide cores whereupon gas from the stellar wind can condense to dust grains, which would lead to an enhanced visibility of the dust debris disks of some giants.

Jura's search was limited to bright giants, for which IR excesses can reliably be determined from the IRAS Point Source Catalogue Version 2 (PSC). Since the IRAS Faint Source Catalogue Version 2 (FSC), has become available, it has become possible to extend the search for IR excesses around late-type giants to a much larger sample. A first glance at the FSC shows that a significant number of excess stars indeed exists (Sect. 2), so that we embarked on a systematic study of this phenomenon. This study is described in Sect.3. During our search, we became aware of an independent study by Zuckerman et

Send offprint requests to: H. Plets

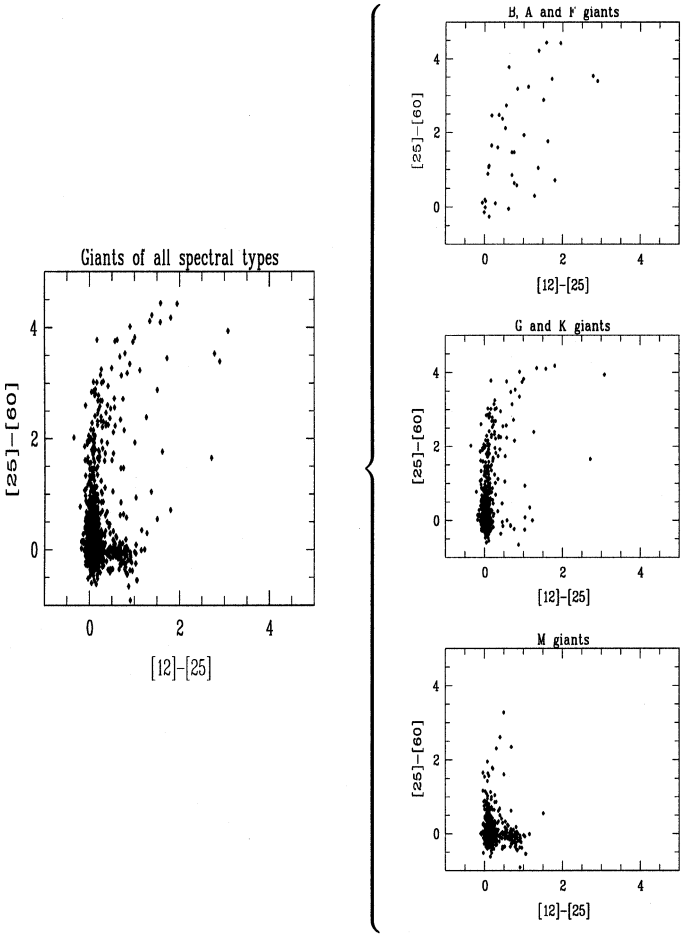

Fig. 1a-d. IRAS two-colour diagram for giants left: **a** Giants of all spectral types; right: **b** B, A and F giants (above); **c** G and K giants (middle); **d** M giants (below)

al. (1995), which contains several objects in common with the present study, but which differs from it on several points we allude to in the text.

2. FSC observations of giants

In studying far-infrared properties for a number of stars, the IRAS colour-colour diagram, in which the [25] − [60] colour (see Eq. (3)) is plotted against the [12] − [25] colour (see Eq. (2)), has proved to be an adequate tool. Since van der Veen and Habing (1988), it has been customary to divide this two-colour diagram into several regions.

We have selected from the FSC all objects which are associated with giant stars which were classified as such from previous optical studies; the details of this selection are outlined in the next section.

In Fig. 1a we display the IRAS colours for the objects for which the FSC lists a flux quality number of 2 ('moderate') or 3 ('good') at 12, 25 and 60 μ (for most objects, the FSC only gives an upper flux limit (flux quality 1) at 100 μ; we discuss the information at 100 μ in a forthcoming paper). An overwhelming majority of these objects are found near the Rayleigh-Jeans point, i.e. $c_{12} \equiv [12] - [25] < 0.4$ and $c_{23} \equiv [25] - [60] < 0.3$ (Oudmaijer et al. 1992), but several objects with excesses are observed. It is striking that these excess objects mainly occur in the region labeled "VIa" by van der Veen and Habing (1988), which means that they have excesses at 60 μm, but hardly so at 12 and 25 μm.

By imposing that the flux quality has to be at least 2 in all three bands, we certainly created a very biased sample. Due to the relatively poor sensitivity of IRAS, only the brightest objects can be seen photospherically at 60 μm. So, extracting a sample only consisting of objects with a moderate or good 60 μm flux quality gives an unrealistically high fraction of giants with excess emission at 60 μ. The IRAS colour-colour diagram thus demonstrates that excesses are observed, but does not enable us to derive in what fraction of the stars this phenomenon occurs.

It is appropriate to investigate whether this high population level of region VIa is caused in the same amount by stars of all spectral types or rather by objects within a specific spectral range. We have therefore divided the giants according to their spectral type: the first group consists of B, A or F (hereafter BAF) giants (Fig. 1b), the second one of G or K (hereafter GK) giants (Fig. 1c) and the third of M giants (Fig. 1d).

The BAF giants are mostly too hot to be detected photospherically at 60 μm by IRAS. So, apart from the objects with very high visual brightness, the early-type giants in Fig. 1b are excess stars. They do not cluster in region VIa, but appear to be scattered throughout the colour-colour diagram. Therefore, apart from objects with very high visual brightness, we only select excess stars, and rather few of them. So, it appears that the BAF giants cannot be held responsible for the 60 μm excess feature in the colour-colour diagram of Fig. 1a.

It can be seen from Fig. 1c. that especially the GK giants lay at the origin of the phenomenon. Fig. 1d. contains a similar amount of objects as Fig. 1c. Most of these M giants appear to cluster around the Rayleigh-Jeans point; some do present a (rather small) 60 μm excess, while others show hotter (25 μ) excesses.

It is a remarkable fact that excesses are observed most often at 60 μm and less so at shorter wavelengths, despite the fact that the selection of shorter-wavelength excesses is favoured observationally. Fig. 1c therefore strongly suggests the existence of giants with excess emission essentially starting beyond 25 μm. As already mentioned above, a thorough discussion of the 100 μm excesses of these stars is hampered by the lack of 100 μ information provided by IRAS, whose detection limit is much lower at this wavelength.

In the following sections, we will investigate the incidence of the phenomenon into some more detail, taking into account the various selection effects imposed by the selection of the sample.

3. Detailed description of the sample

3.1. Data sources

Since we want to investigate the IR excesses of giants as a function of spectral type, we need accurate spectral classifications. When possible, i.e. for the part of the sky with declination up to $-12°$, we relied on the Michigan Spectral Catalogue (MSC), Volumes 1-4 (Houk et al. (1975-1988). For the part of the sky with $\delta > -12°$, we limited our study to stars contained in the Bright Star Catalogue (BSC), 5th edition (Hoffleit and Warren 1991). To be considered as a giant, the spectral identification in BSC or MSC has to contain luminosity class II-III, III, (III) or III-IV, or the BSC spectral type has to contain the prefix 'g'. We point out that the visual magnitude limit of the northern stars in our sample is therefore intrinsically brighter than for the southern ones, but this difference turns out to be hardly significant when only objects detectable by IRAS are considered (see below).

As far as the IRAS-data of those stars are concerned, we use the PSC as well as the FSC to extract the far-infrared fluxes. We have then cross-correlated MSC and BSC with PSC and FSC, using the Associations Table Version 2.0 of the PSC (1987) (Assocpsc) and the Associations Table of the FSC (1990) (Assocfsc). We omitted infrared sources for which an association with more than one optical source was given. E.g. IRAS F04411-0853 is associated to both HR1505 and HR1506, a spectroscopic binary system and is thus not included in our sample.

Some numerical results of this cross-correlation are listed in Table 1. The second and third column give the absolute and relative numbers of BAF, GK and M giants found from the optical sources. The number of those contained in the Assocfsc is listed in column 4, whereas the corresponding fraction is given in the fifth column. In columns 6 and 7, the same is done with with respect to the Assocpsc.

The higher fraction of M giants detected in the PSC reflects the higher detection limit of this catalogue. Indeed, since the PSC contains much more sources than the FSC, which excludes sources near the Galactic plane, it could be expected that the former supplies us with more sources for all spectral types. This is, however, not the case, because the FSC looks roughly one magnitude sharper than the PSC. Only for the reddest stars, like the M giants, the PSC produces the largest sample. On the other hand, the more massive early-type giants are also underrepresented in the FSC, because this survey does not include sources located within $10°$ from the galactic plane. Since not only the number of GK giants is larger in the Assocfsc, but the FSC-fluxes also tend to be more conservative (i.e. lower) than the PSC-fluxes for sources detected both in FSC and PSC, we discuss here the analysis for the FSC data.

Undoubtedly, there is a number of IRAS-detected giants that are not listed in the Assocpsc or Assocfsc, because the association was too uncertain.

3.2. The sample of giants detected at 12, 25, and 60 μm

As seen from Table 1, we started with a sample of 49844 giants, taken from MSC and BSC, and lost about 2/3 of them after correlating the sample with the Assocfsc, leaving us with 17896 objects. We now want to select only stars with FSC flux quality 2 or 3 measurements in all three bands. Only 1713 objects comply with this requirement. We thus loose $\sim 90\%$ of the correlated sample and even $\sim 97\%$ of the original optical sample.

A simple calculation leads us to the estimation that we miss some 1000 good candidates because of the lack of MSC information in the region of the sky with $\delta > -12°$. Indeed, from the part of the sky with $\delta \leq -12°$, we have 1073 MSC sources of which 430 (40 %) are also BSC sources. Since we find 638 BSC sources of the sky with $\delta > -12°$, we can extrapolate there would be 1592 MSC sources with of the sky with $\delta > -12°$, or 954 additional giants. This argument is only valid if these giants are uniformly distributed in space,which seems to be the case: a uniform distribution would imply that 57 % of the objects lie in the region with $\delta > -12°$. In total, we find 1068 well-detected BSC giants, 638 (60 %) of which have $\delta > -12°$.

3.3. The sample of giants with 60 μm excess

The next step is to propose a criterion an object should fulfill to be considered as a giant with 60 μm excess. We make use of the following definitions.

First of all, we use the following expression for the conversion of the (not colour-corrected) fluxes into magnitudes (e.g. Oudmaijer et al. 1992)

$$[\lambda] = m_\lambda = 2.5 * \log \frac{K_\lambda f_\nu[0.00mag]}{f_\nu}, \quad (1)$$

with m_λ the magnitude at wavelength λ, $f_\nu[0.00mag]$ the flux density in Jansky corresponding to the zero magnitude, as given by the IRAS Explanatory Supplement (1985), K_λ the colour correction factor and f_ν the flux in Jansky. The colour-correction factors to a 5000 K black body are 1.43, 1.40, 1.32 and 1.09 at 12, 25, 60 and 100 μm, respectively, resulting in zero magnitude flux densities, $K_\lambda f_\nu[0.00mag]$, of 40.5, 9.42, 1.57 and 0.47 Jansky.

Next, for the calculation of the infrared colours:

$$\begin{aligned} c_{12} &= [12] - [25] \\ &= 2.5 * \log(\frac{K_{12} f_{12}[0.00mag]}{K_{25} f_{25}[0.00mag]} \frac{f_{25}}{f_{12}}) \\ &= 2.5 * \log(\frac{40.5}{9.42} \frac{f_{25}}{f_{12}}) \end{aligned} \quad (2)$$

and

$$\begin{aligned} c_{23} &= [25] - [60] \\ &= 2.5 * \log(\frac{K_{25} f_{25}[0.00mag]}{K_{60} f_{60}[0.00mag]} \frac{f_{60}}{f_{25}}) \\ &= 2.5 * \log(\frac{9.42}{1.57} \frac{f_{60}}{f_{25}}) \end{aligned} \quad (3)$$

Table 1. Results from the cross-correlation between optical and infrared sources.

Spectral	Optical sources		Assocfsc		Assocpsc	
group	number	fraction	number	fraction	number	fraction
BAF	10701	21%	518	3%	315	2%
GK	35824	72%	15061	84%	9923	77%
M	3319	7%	2317	13%	2797	21%
Total	49844	100%	17896	100%	13035	100%

Table 2. The well-detected sample and its excess sources.

Spectral group	# Well-detected objects	# excesses	fraction (in %)
BAF	38	7	18
GK	839	224	27
M	836	83	10
Total	1713	314	18

A 60 μm excess is then defined in following manner:

1. The quoted flux densities should be of sufficient quality. We therefore accept only objects with flux quality at least 2 at 12, 25 and 60 μm. This requirement was already incorporated in the sample defined in the previous section.

2. Excess stars are the ones located outside the Rayleigh-Jeans point of the ($[12]-[25], [25]-[60]$) colour-colour diagram. Of the excess stars, we want to filter those with only 60 μm excess. Therefore, we require

$$c_{12} < 0.4 \tag{4}$$

$$c_{23} > 0.4, \tag{5}$$

where in Eq. (5) a possible error of 0.1 mag. was incorporated. The results are summarised in Table 2.

As can be seen in Table 2, our correlation between MSC and BSC on the one hand and Assocfsc and FSC on the other hand, provided us with 224 GK giants with infrared excess. We performed the whole procedure again, replacing Assocfsc and FSC by Assocpsc and PSC. We thus found 60 new members, adding up to 284 GK giants. These new members lie mostly in the galactic plane, which explains why they weren't included in the sample based on the FSC.

Other excess stars can be found when relaxing the criterion that only GK giants with a quality flag of 2 or 3 in all three bands are considered, i.e. objects with well detected 60 μm fluxes but with only upper limits at 12 and/or 25 μm. Clearly, all such objects show a 60 μm excess. We thus found another 80 GK giants. Our master list, which can be consulted[1], thus contains 364 GK giants with far-infrared excess emission.

[1] The master list is written in the file dist/hansp/masterlist which can be retreived via anonymous ftp at hubble.ster.kuleuven.ac.be (134.58.55.8)

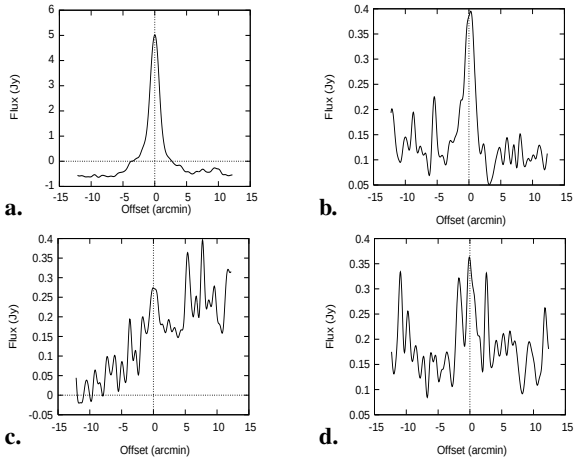

Fig. 2. a 60 μm scans for typical sources of class I, **b** class II, **c** class III and **d** class IV

The large number of GK giants in this masterlist justifies further, more detailed, investigation of this phenomenon. For this scope, it might be better to extract the most interesting and convincing members from this list. We therefore studied the individual 60 μm IRAS scans for each of the 284 GK giants fulfilling our criterium. This enables us to check the degree of reliability of the detections. For this purpose, we used GIPSY, the Groningen Image Processing SYstem (Van der Hulst et al. 1992). With SCANAID we made one-dimensional co-adds and with IMAGE two-dimensional ones. The members were then classified into four classes, according to the quality and reproducibility of the scans: Class I consists of the most reliable sources, i.e. (nearly) all individual scans show a clear signal at the source position; class II objects are detected in typically $\sim 50\%$ of their individual IRAS scans; class III objects are detected in less than half the scans; class IV contains the objects with the lowest scan qualities. For each class, a typical scanaid output, i.e. the mean of all the individual scans, is shown in Fig.2a-d. The diagrams have the offset (in arcmin) in abscissa and the flux density (in Jy) in ordinate. Based on these scans, we calculated the fluxes with the GIPSY-software, in order to find out whether the FSC-fluxes are reliable. In most cases, we found the same flux. In the few other cases, the flux derived with GIPSY was even higher than the FSC-flux. We thus conclude that the detections are not spurious.

Table 3. The four classes based upon scanaid results.

Class	number of members	fraction (in %)
I	65	23
II	49	17
III	68	24
IV	102	36
Total	284	100

The results of this classification are listed in Table 3. In Appendix A and B we list the class I and class II objects, together with their spectral type and 60 μm excess.

Zuckerman et al. (1995) also discuss luminosity class III stars with excess far-infrared emission. They report that their analysis resulted in some 300 giant stars with associated dust. In their letter, they list the 92 'best candidates' of these, 84 of which belong to spectral types G or K. Whereas we composed a sample by restricting ourselves to pure 60 μm excess giants, Zuckerman *et al.* also allowed giants with 25 μm excess. In this manner, 18 objects in the list of Zuckerman were not selected in our list. The remaining 66 GK giants in the sample of Zuckerman were also found in our sample. As could be expected from the fact that they publish only the best candidates in their letter, most of these sources belong to class I.

3.4. Magnitude-limited sample

In this paragraph, we discuss the frequency of the 60 μm excesses among GK giants. For A-type main-sequence stars, the Vega-phenomenon is generally believed to occur at a frequency of (at least) 20% (e.g. Aumann 1988). The best way to estimate the frequency is to select a sample containing only those GK giants that should be detected photospherically at the relevant IRAS bands. Unfortunately, statistical studies of this kind are fairly difficult to perform with the IRAS-sensitivity: as we will show below, only a small fraction of our optical selection of giants are reliably detected in the 12, 25, and 60 μm bands; the sample of giants detected at 100 μm is much lower still. The maximal visual magnitude at which a star of a given spectral type should be detected is listed in Table 4. It was determined as follows. For each spectral subtype, a mean $B-V$ can be found (e.g. Zombeck 1990). This $B-V$ is related to $V-[12]$ by the following equation (Waters et al. 1987)

$$V-[12] = 0.05 + 3.13(B-V) - 1.26(B-V)^2 + 0.29(B-V)^3 + 0.16(B-V)^4. \quad (6)$$

We thus obtain a typical $V-[12]$ for each spectral subtype. With the colour-corrected relations between the IRAS colours (Oudmaijer et al. 1992),

$$[12]-[25] = 0.00 \quad (7)$$

and

$$[25]-[60] = 0.05, \quad (8)$$

we can calculate $V-[25]$ and $V-[60]$. Equation (6) is valid for giants, provided $-0.25 < (B-V) < 1.60$. This condition was met by all sample objects. We also checked the validity of this equation by considering a sample of 555 giants in the Rayleigh-Jeans region of the colour-colour diagram. The predicted photospheric fluxes, calculated with the above equations were on the average within 3% of the observed fluxes.

Adopting an average value of 0.2 Jy for the FSC 90% completeness limit, the above equations then yield the limiting apparent visual magnitude for [12], [25] and [60] (Table 4). So all giants brighter than these limits should have been detected photospherically by IRAS. It can be deduced from the second column of Table 4 that the maximal visual magnitude to be detected at 12, 25 and 60 μm is below 6.5 for all spectral types. This implies that the BSC is a complete catalogue as far as stars without excesses are concerned. We therefore only considered giants listed in the BSC for the construction of this magnitude-limited sample. On the other hand, for giants later than K0 the BSC sample may miss some objects that have excesses at 60 μm but not at shorter wavelengths. In the fourth column, the number of objects with an FSC quoted flux quality which is greater than 1 (i.e. moderate or good quality) at 60 μ is given.

For the K giants, we find a 60 μm excess frequency of $\approx 8\%$. The slight differences between the number of selected objects (column 3) and the number of objects with $fq_{60} > 1$ is due to the fact that we adopted a mean $B-V$ value for each spectral subtype and because we choose an average value (0.2 Jy) for the FSC detection limit, whereas it actually depends on the local background. It is, for instance, possibly that a source with a flux of 0.25 Jy is not detected because it is seen in projection against a rather turbulent background.

A next step in this analysis is to find a relation between the excess fraction and the spectral subclass. Although for most spectral subclasses the data are too scarce, Table 4 suggests that the fraction of excess peaks around K3-K5.

In his paper, Jura (1990) selected K and G giants from the BSC (4th edition) but with apparent visual magnitude less than 4.0 mag. He thus selected 44 G giants and 101 K giants. From those, he finds 37 G giants and 85 K giants with useful IRAS PSC measurements. In this manner, of the 2569 K or G giants in the BSC only 122 (5%) are considered. Jura detected no G giants with 60 μm excess. For the K giants, he finds six possible excesses, three of which were rejected because these stars lie too close to the galactic plane. Thus having left over only three objects, he refrained from calling this finding statistically relevant. These results can now be compared with those of our magnitude-limited sample, described in Section 3.4. The absence of excesses among G giants is in agreement with Table 4. As far as the K giants are concerned, there is a discrepancy between the results of Jura and those in Table 4: 3 excesses versus 29. This is fully due to the fact that Jura adopts a value of 4.0 mag as limiting magnitude. When we apply our criterion, we even find only one single K giant brighter than 4.0 mag with excess instead of six. Indeed, three of them are not included in the FSC because, as mentioned above, they lie near the Galactic plane; one other has a bad flux quality in the FSC; for one star

Table 4. Detection limit on the V-magnitude for the three IRAS bands as a function of spectral type. *Remark:* The third column excludes objects within the Galactic plane and objects without a sufficiently accurate IRAS association.

Spectral Type	V_{lim}	#objects	# fq$_{60}$ >1	# excesses	$\frac{\#excesses}{\#objects}$ (in %)
G0-G5	4.49	6	6	0	0
G8	4.55	17	16	0	0
K0	4.74	28	25	2	7.1
K1	4.88	24	18	0	0
K2	5.01	24	20	1	4.2
K3	5.37	56	47	6	10.7
K4	5.69	65	58	7	10.8
K5	6.16	116	97	7	6.0
M0	6.20	47	45	0	0
M1	6.21	44	42	1	2.3
M2	6.32	55	53	0	0
M3	6.36	44	43	0	0
M4	6.32	26	26	0	0
M5	6.13	12	12	0	0

the FSC-flux is lower than the PSC-flux, so that the c_{23} based on the FSC-data does not exceed the limiting value of 0.4 mag. The main reason why only the visually brightest stars were allowed by Jura to enter the target list, is because the author was very much concerned with the problem to disentangle eventual excess fluxes from photospheric fluxes. But in fact, the uncertainty on the photospheric fluxes hardly does affect our results, since the photospheric fluxes at 60 μm are small anyway. We therefore conclude that Jura's conclusion that there is absence of circumstellar dust debris around G giants was affected by the fact that his sample suffers from small-number statistics.

3.5. The complete sample

The classification of the magnitude-limited sample into spectral subclasses in Table 4 did not permit to draw robust conclusions about the distribution of the excesses over the distinct spectral subclasses. Therefore, we made a similar analysis with the sample containing all excess giants.

We determined the excess fluxes in Jansky according to the scheme outlined in Section 3.4. For all excess GK giants the $(B-V)$ and V of which is known, we calculated the expected photospheric 60 μm magnitude, using Equation (6), Equation (7) and Equation (8). We then converted this 60 μm magnitude into the expected photospheric 60 μm by rewriting Equation (1) as

$$(f_\nu)_{phot} = K_\lambda f_\nu[0.00mag]10^{-\frac{m_\lambda}{2.5}}. \quad (9)$$

The 60 μm excess, E_{60} was than simply defined as

$$E_{60} = (f_{60})_{FSC} - (f_{60})_{phot} \quad (10)$$

For the members of our masterlist for which a reliable $B-V$ is known, we thus calculated the 60 μm excess fraction, i.e. the ratio between E_{60} and $(f_{60})_{phot}$. The results are listed in Table 5.

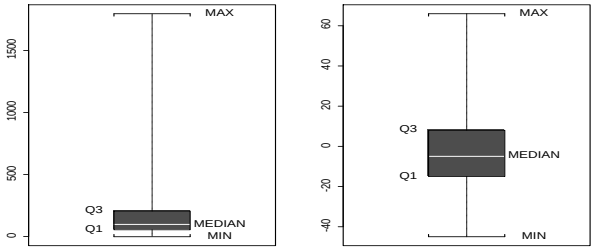

Fig. 3a and b. Boxplots: Q1 and Q3 are, respectively, the first and the third quartile (see Appendix C). The ordinate represents the ratio between the excess flux and the predicted photospheric flux, expressed in %. **a** the selected sample (left). **b** a sample of Rayleigh-Jeans giants (right).

We conclude that
1) the phenomenon starts beyond G4;
2) the fraction of excess remains more or less constant between G5 and K4;
3) it then peaks at spectral subtype K5;
4) the fraction of excesses at spectral subtypes of M remains relatively high.

Probably, then, the smaller fraction of excess stars among the M giants in Table 2 is a selection effect, due to the fact that the photospheres of M giants are detected for fainter stars.

In Fig.3 we show a boxplot [2] of these excess fractions (a), compared to a sample containing only giants in the Rayleigh-Jeans region of the colour-colour diagram (b).

Since we calculate the excess fraction, i.e. divide by the predicted photospheric flux, the giants with very small predicted photospheric fluxes are left out from the boxplot. The concept of boxplots enable a direct visual interpretation of the data. From Fig.3, one can immediately see that the Rayleigh-Jeans

[2] see Appendix C for a brief description

Table 5. 60 μm excesses among G, K and M giants (based on FSC data)

Spectral Type	# objects	# associations	# excesses	$\frac{\#\,excesses}{\#\,assoc}$ (in %)
G0-G4	318	79	0	0.0
G5-G7	2081	466	12	2.6
G8-K0	14178	5348	99	1.9
K1	8495	2743	44	1.6
K2	5419	2855	49	1.7
K3	2807	1837	41	2.2
K4	1336	959	26	1.9
K5	1070	748	29	3.9
M0	557	382	9	2.4
M1	837	577	20	3.5
M2	821	585	23	3.9
M3	561	396	20	5.1
M4-M5	441	305	13	4.3
M6-M8	99	71	4	5.6

sample is almost symmetrically distributed (3b), whereas the excess sample is right-skewed (3a), i.e. the upper 50 % of the data points span a much greater range than the lower 50 %, or, alternatively, the distribution trails off more slowly on the right side than on the left side.

If no excesses are expected, the spread in the data can be ascribed to observational errors. A Gaussian distribution is then expected. For the Rayleigh-Jeans sample, we find indeed a distribution which is close to Gaussian, whereas the excess sample rather follows a lognormal distribution, indicating that the excesses are genuine. It can be deduced from the boxplot that most of the excesses are sufficiently high, the median being 98 % and the mean 193 %. So, there is no danger that our excesses are within the error bars of the observed and predicted fluxes, in agreement with the conclusion for the magnitude-limited sample. It also shows that the excess criterium we used is adequate. The sample of giants within the Rayleigh-Jeans region have a mean excess of -2.5 % and a median of -5 %. The third quartile of this Rayleigh-Jeans sample has an excess fraction of only 8 %. So, since the uncertainty on the photospheric fluxes is of the order of 10 % (Waters 1987) and the uncertainty of the observed fluxes often exceeds 10 %, we can conclude that our criterium to select excesses, as expressed in Eq.(4) and Eq.(5), is reliable.

Nevertheless, the Rayleigh-Jeans sample seems to contain a few excesses. They can be ascribed to giants with comparable excesses at 12, 25 and 60 μm.

3.6. Additional analysis

3.6.1. Survival analysis

Apart from the analysis of the magnitude-limited sample, as described in Section 3.4 and the analysis on the whole sample. as described in Section 3.5, we also considered an alternative statistical approach to the problem of the frequency of the excesses by applying the methods of survival analysis. The underlying principle is that censored observations, like upper flux limits in our case, do contain (partial) information (e.g. Miller 1981). A function S, the *survival function*, is defined as

$$S(x) = P(X > x), \tag{11}$$

denoting the probability that a random variable X exceeds a given value x. In our case, we want to know the probability that $c_{23} > 0.4$ for the distinct spectral subtypes. Using the Kaplan-Meier product-limit estimator (e.g. Miller 1981), we obtained the results listed in Table 6. We will elaborate on this a forthcoming paper.

Table 6. Kaplan-Meier estimator for the survival function for several spectral subtypes.

Spectral Type	$\widehat{S}(c_{23}) > 0.4$ expressed in %
G8	8
K0	19.5
K1	25
K2	9
K3	21
K4	11
K5	6.5
M	2.2

3.6.2. Spatial extent

In order to determine the spatial extent of the excess radiation, we have compared the SCANAID profiles of the programme stars with those of point sources such as β Gru and γ Dra. In Fig.4 we show the profile of γ Dra superposed on that of the sources HD30834, which has a very large excess, and HD97866. In the former case, it is clear that the source is extended, while the latter star is a point source at IRAS resolution. It appears

Table 7. Extended sources

HD	Spectral type	b	image co-added info	remarks
30834	K2.5IIIbBa0.4	-4.65	no contamination	Li-rich
60341	K0III	+0.06	contamination	
107446	K3/4III	+2.25	contamination ?	Variable Star
146850	K3IIICNVP	+24.44	contamination ?	Li-rich
152786	K3III	-8.20	no contamination	
164358	K5III	+2.85	contamination	
167818	K3III	-5.29	contamination ?	
176884	KOII/III	-11.12	no contamination	Star in double system
202320	K0II/III	-40.61	contamination ?	

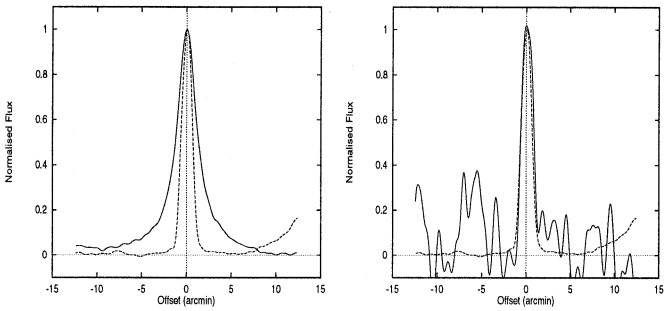

Fig. 2. a γ Dra (dotted) and HD30834 (full) (left); **b** γ Dra (dotted) and HD97866 (full) (right)

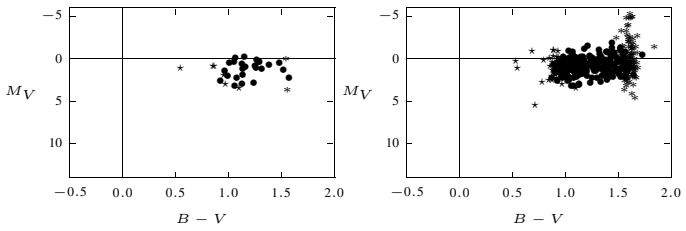

Fig. 5a and b. Observational HR-diagram of **a** G, K and M giants with infrared excess with known parallax (left); **b** all G, K and M giants with known parallax (right). Legend: $\star$: G giants; $\bullet$: K giants; $*$: M giants.

that the large majority of giants with excesses are unresolved. We found only eight other sample stars with an extent similar to HD30834 (see Table 7). Viewing two-dimensional co-added images of the stellar field around each of these nine extended sources reveals that three of them, HD30834, HD152786 and HD176884, seem to be genuinely extended, i.e. not affected by cirrus.

4. Discussion

The main results of our investigation can be summarized as follows. We confirm the discovery by Zuckerman et al. (1995) that giants with infrared excesses exist (with an estimated frequency of $\approx 8\%$), but that they are less common than Vegatype stars ($\leq$ 20%), a result anticipated by Jura (1990); the excesses appear at spectral type G5 and from there on involve a rather constant fraction of stars; the circumstellar material is very cold, i.e. only few 25 μm excesses are observed; except for a few cases, the excess objects appear point-like at the IRAS wavelengths.

Before discussing the possibility that the excesses have the same origin as those of the Vega-like objects, it is appropriate to investigate other hypotheses, such as the presence of circumstellar matter due to mass ejection by the giant. Mass loss is known to occur from AGB stars, and leads to important infrared excesses once luminosities of the order of $M_V \approx -1.4$ (i.e. the absolute visual magnitude for Mira) are attained. For a relatively large fraction of the giants in this study, the parallax is known. In Fig. 5a we display these objects in the observational HR diagram; the data are taken from the Hipparcos Input Catalogue Version 2.0 (Turon et al. 1993); since it concerns nearby stars, the reddening can be neglected.

It can be seen on the figure that all stars with excesses for which a parallax is known are less luminous than about M_v = 0.0. In fact, it turns out that these objects cover the full domain in the HR diagram that is defined by all giants in the Hipparcos Input Catalog (see Fig. 5b). We conclude, therefore, that the giants with infrared excesses essentially all are first-ascent giants, and thus that the sample is not significantly affected by the presence of asymptotic giant branch stars.

Whether first-ascent red giants are also subject to mass loss, can be inferred from the fact that RR Lyrae stars consistently have lower masses than the highest initial mass for a star that cannot yet have left the main sequence in a Hubble time. How and when red-giant mass loss occurs is not well known. For AGB stars, the current idea is that mass loss is a discontinuous, recurring phenomenon, probably connected with the thermal pulse phase (Zijlstra et al. 1992). However, we consider it unlikely that the excesses we observe are due to mass loss. First, it is most likely that most of the mass is lost at the Helium flash; if that were the circumstellar mass we observe, one would expect that the distribution of our stars in the HR diagram is more clumpy than on Fig. 5a. Second, one of the striking characteristics of our stars, is that their IR excesses occur essentially at larger

wavelengths, indicating detached shells, and so are difficult to reconcile with recent mass loss.

Since in addition there is no evidence that a larger than average binarity occurs in the giants with excesses, it then seems most natural to conclude that the excesses are of a similar nature than those observed in Vega-like stars. By all means, the fraction of excess stars among giants is distinctly smaller than among main-sequence stars. It is tempting to attribute this, as Jura (1990) did, to the evaporation of the circumstellar debris due to the higher radiation field of the giant. On the other hand, it has to be said that little is known about the evolution of the fraction of Vega-like stars on the main sequence. The smaller fraction of giants with excesses may also be partly due to the gradual destruction of the circumstellar bodies and the subsequent decrease of the likelihood of collisions.

Acknowledgements. We thank Dr. C. Vynckier for helping us with the statistical analysis.

Appendix A: list of class I objects

HD	Spec. Type	E_{60}	fraction
6	gG9	0.27	4.89
3574	K7 III	0.05	0.08
3627	K3 III	1.16	0.88
5384	K5 III	0.28	1.15
9362	K0 IIIB	0.18	0.47
9408	G9 IIIb	0.60	3.16
23978	K5 III	0.22	0.58
25604	K0+III-IIIaFe-0.2	0.10	0.32
30504	K3.5 III	0.37	0.82
30834	K2.5 III	5.98	13.0
31296	gK1	0.13	0.75
31553	gG8	1.23	14.0
32406	K0 II/III	0.63	7.88
32440	K4 III	0.22	0.63
33419	K0 III	0.38	5.79
34043	gK4	0.38	1.77
36597	K1 II/III	0.30	0.55
43827	K1 III	0.50	2.03
48674	K0 III	0.46	23.0
52904	K4 III	0.23	3.54
60341	K0 III	1.26	12.6
61949	K4 III	0.47	5.22
66075	K3 III	*	*
76236	K5 III	0.37	1.11
78004	K2 III	0.36	0.53
82227	K1 III	0.38	19.0
82421	K0 III	0.51	17.0
92253	K0 III	0.61	30.5
97472	K2/3 III	0.56	5.77
97866	K4 III	0.05	0.22
102040	K2/3 III+A	0.64	12.8
104555	K3 III	0.31	2.93

continued on next page

continued from previous page

HD number	Spectral Type	E_{60} (Jy)	excess fraction
107446	K3/4 III	0.75	0.52
112570	K0 III/IV	0.18	3.34
114287	K5 III	0.36	1.80
118344	K3 III	0.64	4.57
129456	K3 III	1.47	1.92
138688	K2/3 III	1.20	4.92
139997	K5 III	0.97	1.22
143619	K2/3 III	1.40	12.5
145206	K4 III	0.25	0.82
145449	K1 III	0.77	25.7
146850	K3 III	1.92	8.61
152786	K3 III	1.8	0.46
153135	K2 III	0.79	19.8
153639	G8 III	3.69	48.2
153687	K4 III	4.74	8.63
156115	K5 III	0.56	1.60
162298	K4 III	0.40	8.00
164358	K2 III	1.35	2.81
166063	K0 III	0.47	2.05
167818	K3 III	1.22	0.99
173460	K5 III	0.62	1.27
175775	G8/K0 III	0.19	0.23
176884	K0 II/III	1.65	15.8
179886	K3 III	0.29	1.30
190299	K4 III	0.27	1.79
202320	K0 II/III	0.49	2.97
202418	K3 III	0.80	8.32
211073	K3 III	0.42	0.73
212320	G6 III	0.61	9.82
218559	K4 III	0.47	3.51
221776	K7 III	0.73	3.34
223559	K4 III	0.43	1.62

Remark: for HD 66075 no photometric data were found.

Appendix B: list of class II objects

HD	Spec. Type	E_{60}	fraction
15694	K3 III	0.07	0.35
19080	K3 III	0.13	1.21
26038	K5 IIIb	0.17	0.79
27693	G8 III	0.17	8.74
41927	K1.5 IIIb	0.08	0.33
42341	K2 III	0.15	1.23
50002	K3 III	0.09	0.83
55526	K2 III	0.12	0.53
56813	K4 III	0.17	0.74
58776	K2 III	0.35	28.5
63744	K0 III	0.14	0.63
68298	K4 III	0.96	28.6
70264	K2 III	0.28	6.11
70647	K5 III	0.22	0.83

continued on next page

continued from previous page

HD number	Spectral Type	E_{60} (Jy)	excess fraction
71176	K4/5 III	0.14	0.38
72066	K3/4(III)	0.90	12.6
74006	G5 II/III	0.10	0.31
76376	K2/3 III	0.16	1.09
76579	K3 III	0.10	0.41
82870	K1 III	0.06	0.49
83240	K1 III	0.11	0.68
86378	K5 III	0.17	0.59
88333	K2 III	0.13	0.81
91190	G8.5 III	0.07	0.47
92770	K3/4(III)	0.09	0.50
96301	K5 III	0.30	26.3
97907	K3 III	0.11	0.70
99322	K0 III	0.12	1.05
110372	K1/2 III	0.45	6.91
129972	G8.5 III	0.07	0.33
131918	K4 III	0.11	0.36
134505	G8 III	0.24	0.44
135291	K2 III	0.48	1.85
139266	K2 III	0.14	12.5
145001	G8 III	0.11	0.91
156266	K2 III	0.09	0.37
159605	K0 III	0.15	18.1
160516	K3(III)	0.57	6.75
161193	gK0	0.40	6.11
163547	gK3	0.13	0.89
164712	K2 III	0.42	3.81
164871	K2/3 III	0.09	1.30
184398	K2 III+A0V	0.82	14.3
187114	K5 III	0.17	3.79
189695	K5 III	0.15	0.66
190608	K2 III	0.41	2.71
210889	K2 III	0.09	0.64
221148	K3 III	0.12	2.26
223647	G6/8 III	0.09	0.77

Appendix C: the boxplot

A boxplot provides information on the location, spread, skewness, tail length and outliers of a data set. It is a powerful exploratory tool, especially when several data sets are to be compared simultaneously. Boxplots replace the more often used histograms, which are very much biased by the choice of the bin size (Tukey 1990). As can be seen from Fig.3, a boxplot depicts 5 quantities: the minimum and maximum value of the data set, labeled *min* and *max*, the first and third quartile, labeled *Q1* and *Q3* and the median. Their meaning is the following. When the data are put in ascending order, the first 25% are located between *min* and *Q1*, the next 25% between *Q1* and the *median*, etc. So, 75% of the data are smaller than the value of *Q3*.

An indication for the spread of the data is given by the *Inter Quartile Range, IQR*, defined as $IQR = Q3 - Q1$. It is the length of the box, containing 50 % of the data. In case of a data set containing outliers, i.e. data points with extreme high or low values in comparison with the bulk of the data, the IQR provides a better indication of the spread than the standard deviation, since the latter can be strongly influenced by outliers.

Table 8. Boxplot parameters for the two samples

Boxplot parameters	Excess sample	Rayleigh-Jeans sample
min	-2.2	-45
Q1	55	-15
median	98	-5
Q3	205	8
max	1796	66
mean	193	-2.5
IQR	150	23

In Table 8, we list the values for these boxplot parameters for both the excess and the Rayleigh-Jeans sample.

More information on boxplots can be found in Tukey (1977).

References

Aumann, H.H., Gillett, F.C., Beichmann C.A. et al.: 1984, ApJ 278, L23,

Aumann, H.H.: 1988 AJ 96, 1415

Backman, D.E., Paresce, F.: 1993 Protostars and Planets III, eds. Levy, E.H., Lunine, J.I., The University of Arizona Press, USA, 1253

Backman, D.E., Dasgupta, A., Stencel, R.E.: 1995, ApJ 450, L35

Edgeworth , K.E.: 1949, MNRAS 109, 600

Fernandez, F.: 1980, MNRAS 192, 481

Hoffleit, D., Warren, W.: 1991, Preliminary Version of the Bright Star Catalogue, 5th Revised Edition, Yale University Observatory, New Haven, USA

Houk, N., Cowley A.P.: 1975, Michigan Catalog of 2-Dimensional Spectral Types of HD stars, University of Michigan, Ann Arbor

Houk, N.: 1978, Michigan Catalogue Of Two-Dimensional Spectral Types For The HD Stars, Volume 2

Houk, N.: 1982, Michigan Catalogue Of Two-Dimensional Spectral Types For The HD Stars, Volume 3

Houk, N., Smith-Moore: 1988, Michigan Catalogue Of Two-Dimensional Spectral Types For The HD Stars, Volume 4

IRAS, FSC: Faint Source Survey Explanatory Supplement, Version 2.0: 1988, Infrared Processing and Analysing Center, Californian Institute of Technology, Pasadena, California, USA

IRAS, PSC: Point Source Catalog, Version 2: 1985, US Government Publication Office

IRAS Catalogues and Atlasses. The Explanatory Supplement: 1985, eds. Beichman, C.A., Neugebauer, G., Habing, H.J., Clegg, P.E., Chester, T.J., NASA RP-1190, Government Printing Office, Washington, D.C.

Jura, M.: 1990, ApJ 365, 317

Kuiper, G.P.: 1951, Astrophysics, eds. Hynek J.A., 357

Matese J., Whitmire, D.: 1989, Icarus 81, 24

Miller, R.G., Jr. 1981, Survival analysis, J. Wiley & Sons, New York, USA

Oudmaijer, R.D., van der Veen, W.E.C.J., Waters, L.B.F.M., et al.: 1992, A&AS 96, 625

Plets, H.: 1997, Ph.D. Thesis, Katholieke Universiteit Leuven, België (in preparation)
Telesco, C.M., Knacke, R.F.: 1991, ApJ 372, L29
Tukey, J. W.: 1977, Exploratory Data Analysis, Addison-Wesley Reading (Mass.)
Tukey, J. W.: 1990, Data-based graphics: visual display in the decades to come. Statistical Science 5, 327-339
Turon, C., Creze M., Egret D. et al.: 1993, Bull. Inf. CDS 43, 5
Van der Hulst, J.M., Terlouw, J.P., Begeman, K.G., Zwitser, W., Roelfsema, P.R.: 1992, in ASP Conf. series no. 25, eds. D.M. Worall, C. Biemesderfer and J. Barnes, 131
Van der Veen, W.E.C.J., Habing H.J.: 1988, A&A 194, 125
Waters, L.B.F.M., Coté J., Aumann H.H.: 1987, A&A 172, 225
Weissman, P.R.: 1995, ARA&A 33, 327
Zijlstra, A.A., Loup, C., Waters, L.B.F.M., de Jong, T.: 1992, A&A 265, No.1, L5
Zombeck, M.V.: 1990, Handbook of space astronomy and astrophysics, 2nd edn, Cambridge University Press, England, 70
Zuckerman, B., Kim, S.S., Liu, T.: 1995, ApJ 446, L79

This article was processed by the author using Springer-Verlag LaTeX A&A style file *L-AA* version 3.